UDC 539. 4

Failure of $Zr_{50}Ti_{16.5}Cu_{15}Ni_{18.5}$ Amorphous Metallic Ribbon

J. Miškuf,[1,a] K. Csach,[1,b] A. Juríková,[1,c] V. Ocelík,[2,d] V. Bengus,[3,e] and E. Tabachnikova[3,f]

[1] Institute of Experimental Physics, Slovakia Academy of Sciences, Kosice, Slovakia

[2] Department of Applied Physics, Materials Science Centre and Netherlands Institute of Metals Research, University of Groningen, Groningen, The Netherlands

[3] Verkin Institute for Low Temperature Physics & Eng. UAS, Kharkov, Ukraine

[a] miskuf@saske.sk, [b] csach@saske.sk, [c] akasard@saske.sk, [d] v.ocelik@rug.nl, [e] bengus@ilt.kharkov.ua, [f] tabachnikova@ilt.kharkov.ua

The deformation and fracture behavior of $Zr_{50}Ti_{16.5}Cu_{15}Ni_{18.5}$ bulk amorphous metal in the form of a thin ribbon have been determined in tensile test at room temperature. The fracture is localized in a major shear band and the fracture angle between the tensile stress axis and the fracture plane is close to 45°. Fractographic observations have revealed that the fracture surface of the amorphous metallic glass consists mainly of a vein-like pattern morphology. We present a scheme of three zones of fracture surface morphology: progressive smooth sliding region (A), dominating vein like pattern (B), and river-like ripples (C).

Keywords: fracture, bulk amorphous alloy, vein-like pattern.

Introduction. Amorphous metallic alloys in the form of ribbons with thickness less than 50 μm are prepared by rapid melt quenching on a rotating disc [1]. The deformation of metallic glass is inhomogeneous in nature at lower temperatures. Owing to the absence of the long-range order, amorphous metallic alloys exhibit a very high yield stress resulting in a very large accumulation of strain energy [2]. These glasses show very little plasticity under tensile loading. Recently, several multi-component metallic alloys with an excellent glass forming ability have been reported. Reduced cooling rates are sufficient to achieve bulk samples in the amorphous state (e.g., rods a few millimeters in diameter) [3]. We present the fracture surface analysis of an amorphous ribbon prepared from the Zr–Ti–Cu–Ni type of alloy, capable of achieving amorphous structure at lower cooling rates.

Experimental. Samples made from a bulk amorphous alloy with the nominal composition of $Zr_{50}Ti_{16.5}Cu_{15}Ni_{18.5}$ (at.%) were used in the experiments. The 300 μm thick and 3–5 mm wide amorphous ribbons were prepared by rapid melt quenching on a spinning metallic disc. The thickness of the prepared ribbon substantially exceeds the maximum thickness of ribbons prepared from standard amorphous alloys. The amorphous structure of a sample was confirmed by X-ray diffraction. Structure properties were characterized by differential scanning calorimetry (Perkin Elmer DSC 7). Ribbons were fractured by a tensile test on the machine with the stiffness of 10 kN/mm, the deformation rate being $2.6 \cdot 10^{-3}$ s^{-1} at 300 K. A scanning electron microscope Tesla BS340 was used for fractographic observations.

Results and Discussion. A wide temperature region of undercooled liquid state above the glass transition temperature T_g (592 K) up to the crystallization temperature T_x (629 K) is typical for the amorphous alloy $Zr_{50}Ti_{16.5}Cu_{15}Ni_{18.5}$ as demonstrated by the DSC thermogram in Fig. 1. The ribbon samples were loaded under uniaxial tension. The measured fracture stress was 1.53 ± 0.15 GPa which is similar to that reported in [4, 5]. The stress–strain curve for $Zr_{50}Ti_{16.5}Cu_{15}Ni_{18.5}$ at a strain rate of $2.6 \cdot 10^{-3}$ s^{-1} at 300 K under uniaxial tension is shown in Fig. 1 on the right side. Multiple serrations were

observed prior to failure. The origin of the serrated flow in metallic glasses is still unclear, it is definitely related to the formation of shear bands. The formation of the individual shear band is manifested in a single serration and all of the work done in producing the shear band is dissipated as heat [6].

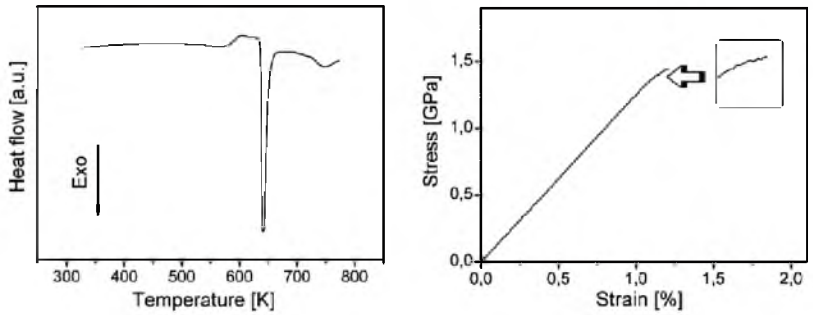

Fig. 1. DSC trace of $Zr_{50}Ti_{16.5}Cu_{15}Ni_{18.5}$ at a heating rate of 20 K/min (a). Stress–strain curve at strain rate of $2.6 \cdot 10^{-3}$ s^{-1} under uniaxial tension at temperature 300 K (b).

The observed macroscopic plastic deformation was just about 0.5%. The fracture is localized in a major shear band and the fracture angle between the tensile stress axis and the fracture plane is close to 45° – the failure in the maximum shear stress plane. The reduced free volume results in the deviation of the shear banding direction from the maximum shear stress [7].

The main fracture surface feature observed was the vein pattern morphology created by the process of meniscus instability [8]. A ridge (vein) on the fracture surface results from a connection of two adjacent cavities that grow under the action of external stress. Such a vein pattern morphology shows a mirror image on two opposite sides of the created fracture surface.

The left side of the fracture surface presented in Fig. 2a shows a vein free area formed during an initial stage of the local shear at the wheel side of the ribbon. This area corresponds to zone *A* of the scheme shown on the right side of Fig. 2. The scheme summarizes all typical features observed on the fracture surface of 300 μm thick amorphous ribbons with a wide undercooled liquid state region and fractured by ductile shear failure.

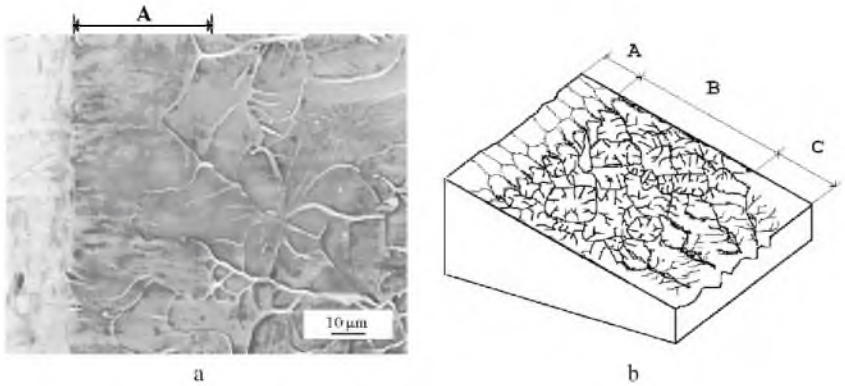

Fig. 2. Fracture surface in the vicinity of a sample edge. An intensive shear near the edge of the fracture surface (a) and the scheme of areas with three characteristic morphologies observed on the fracture surface of a 300 μm thick amorphous ribbon (b).

For standard amorphous metallic alloys in the form of ribbons the failure is initiated mostly at surfaces and only occasionally at extraneous particles or intersections of shear bands [9]. On the fracture surface of a 300 μm thick ribbon we observed the areas with radial veins. These radial veins come out from the central flat area as Fig. 3a clearly shows.

Similar morphology of radial veins was observed on $Zr_{59}Cu_{20}Al_{10}Ni_8Ti_3$ bulk amorphous alloy failed in tensile mode [10]. The fracture nucleates at the central flat part as a consequence of two processes: (i) the nucleation and (ii) the propagation of cores. A subsequent cavity growth proceeds through the formation of radial veins which become finally linked to the main vein around the whole cell – Fig. 3a. The cell contains a flat and radial parts enclosed with secondary vein rings of a cellular unit. No extraneous particles or visible defects are present at flat centers.

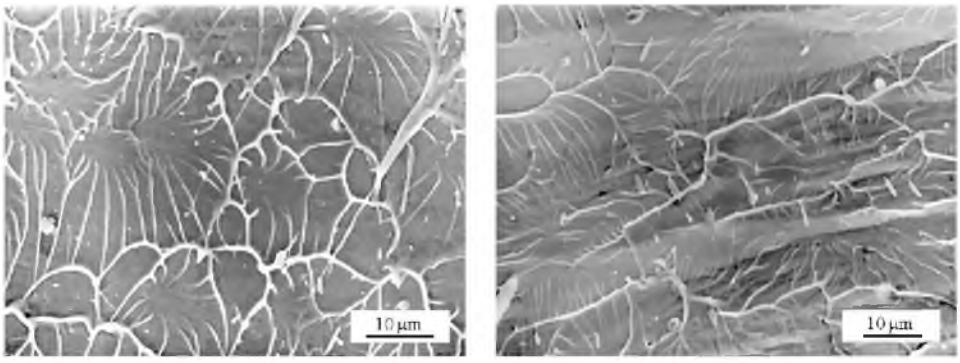

a b

Fig. 3. Cellular vein-like morphology together with areas of radial primary veins – zone *B* (a). "River morphology of fracture surface" corresponding to zone *C* of the scheme in Fig. 2b.

The fractographic analysis of ductile shear failure of a 300 μm thick amorphous metallic ribbon has shown that its morphologic characteristics are close to the features observed on the ductile fracture surface of bulk amorphous metallic materials in a wide variety of forms [9]. The fracture surface is formed through the meniscus instability process inside an adiabatic thin shear band.

A complex stress field at the final fracture stage forms distinct relief structures on the fracture surface with a number of aligned veins. The relief fracture surface contains ridges with the main vein at their tops and ditches between them – Fig. 3b. Aligned primary veins propagate from the rivers to the ridges and link into the main one. This type of the vein organization observed on the fracture surface of $Pd_{40}Cu_{30}Ni_{10}P_{20}$ bulk amorphous alloy is called the river morphology of fracture surface [11]. Similar fracture surface morphology of Zr-based bulk metallic glass matrix composites and Cu-based bulk glass after compression testing was observed in [12]. However, the round cores with radial veins were also observed in compression at elevated temperatures [13].

The tensile failure criterion [14] indicates that tensile failure is controlled by both the normal stress σ and the shear stress τ (where σ_0 is the normal fracture stress and τ_0 is the shear fracture stress):

$$\frac{\sigma^2}{\sigma_0^2}+\frac{\tau^2}{\tau_0^2}\geq 1. \qquad (1)$$

However, the dependence of the shear stress τ on the normal stress σ is not linear as the Mohr–Coulomb criterion. The influence of the normal stress presence during the creation of zones *B* and *C* at failure causes the principal difference in the fracture surface

morphology between zone *A* and zones *B* and *C*. The smooth surface of zone *A* created under the pure shear stress at the first stage becomes, due to increasing normal stress, more multifarious (zone *B*). The increased influence of the normal stress in final stages of deformation and failure and more complex deformation conditions associated with serration on the loading-deformation curve leads to higher surface profile with ripples (zone *C*). Similar distinguishing of fracture stages in the case of a polymer failure was described in [15].

The results suggest that the catastrophic fracture is no longer a pure shear process, whereas the normal stress plays a remarkable role.

Conclusions. The fractographic analysis of the fracture surface of $Zr_{50}Ti_{16.5}Cu_{15}Ni_{18.5}$ amorphous metallic alloy in the form of a 300 μm thick ribbon fractured in tensile tests reveals the presence of shear failure by the meniscus instability mechanism. Features similar to the fracture morphology of bulk amorphous alloys are formed in the catastrophic shear band and presented on the fracture surface.

We have described three different distinct pattern morphologies. Primary progressive sliding in the first region (*A*) is followed by the general fracture that consists of two regions. The presence of the vein-like pattern with frequent radial vein forms is typical of the second fracture region (*B*). The last – third – region of the fracture surface (*C*) has a more pronounced relief and is covered with a river-like pattern. The vein-like pattern of the second region covers a dominant part of the final fracture surface.

Acknowledgment. This work was supported by the Slovak Grant Agency for Science – VEGA.

1. P. Duhaj, P. Svec, E. Majkova, et al., *Mater. Sci. Eng.*, **A133**, 662 (1990).
2. Y. Zhang and A. L. Greer, *Appl. Phys. Lett.*, **89**, art. 071907 (2006).
3. A. Inoue, T. Zhang, and T. Masumoto, *Mater. Trans. JIM*, **31**, 177 (1990).
4. G. Abrosimova, A. Aronin, D. Matveev, et al., *J. Mater. Sci.*, **36**, 3933 (2001).
5. W. Zhang and A. Inoue, *Scripta Mater.*, **48**, 641 (2003).
6. W. J. Wright, R. B. Schwarz, and W. D. Nix, *Mat. Sci. Eng.*, **A319-A321**, 229 (2001).
7. W. H. Jiang, G. J. Fan, F. X. Liu, et al., *J Mat. Res.*, **21**, No. 9, 2164 (2006).
8. F. Spaepen, *Acta Metall.*, **23**, 615 (1975).
9. V. Z. Bengus, E. D. Tabachnikova, J. Miškuf, et al., *J Mat. Sci.*, **35**, 4449 (2000).
10. Z. F. Zhang, J. Eckert, and L. Schultz, *Acta Mater.*, **51**, 1167 (2003).
11. Ch. Ma and A. Inoue, *Mater. Trans. JIM*, **43**, 3266 (2002).
12. M. Kusy, U. Kuhn, A. Concustell, et al., *Intermetallics*, **14**, 982 (2006).
13. G. Wang, J. Shen, J. F. Sun, et al., *Mat. Sci. Eng.*, **A398**, 82 (2005).
14. Z. F. Zhang and J. Eckert, *Phys. Rev. Lett.*, **94**, art. 094301 (2005).
15. J. Fineberg, S. P. Gross, M. Marder, and H. L. Swinney, *Phys. Rev. Lett.*, **67**, No. 4, 457 (1991).

Received 28. 06. 2007